

AERODYNAMIC CHARACTERISTICS OF THE FLOW AROUND AN AIRFOIL AND A CIRCULAR CYLINDER

Mustafa SARIOĞLU*

Mechanical Engineering Department, Faculty of Engineering, Karadeniz Technical University, Trabzon, TURKEY

Geliş / Received: 17.06.2016

Düzeltilmelerin gelişi / Received in revised form: 18.07.2016

Kabul / Accepted: 18.07.2016

ABSTRACT

The flow characteristics around a symmetrical airfoil NACA 0012 at incidence and a circular cylinder placed in tandem have been studied experimentally at a Reynolds number of $1.5 \cdot 10^5$ based on the chord length of the airfoil C . The downstream circular cylinder of diameter $D = 25$ mm used as a bluff body was placed in the same axis in the flow direction in the wake of the airfoil. The dimensionless gap S/D , where S is the longitudinal spacing between the airfoil and the cylinder, and the attack angle of the airfoil, α , were varied from 0 to 4.3 and from 0° to 15° , respectively. The effects of the attack angle of the airfoil and the longitudinal spacing between the airfoil and the cylinder on the pressure distributions and vortex shedding were examined. Characteristics of the vortex formation region and locations of flow attachments, reattachments, and separations were observed by means of the flow visualizations. It has been seen that the airfoil and the cylinder have considerably affected by each other. The variation in the flow structures according to the attack angle of the airfoil and the longitudinal spacing between the airfoil and the cylinder are revealed utilizing the flow visualization photographs.

Keywords: Airfoil, circular cylinder, aerodynamic characteristic, pressure distribution, Strouhal number

BİR KANAT PROFİLİ VE BİR DAİRESEL SİLİNDİR ETRAFINDAKİ AKIŞIN AERODİNAMİK KARAKTERİSTİKLERİ

ÖZ

Ardışık olarak yerleştirilmiş simetrik bir NACA 0012 kanat profili ve bir dairesel silindir etrafındaki akış karakteristikleri kiriş uzunluğuna göre tanımlanmış Reynolds sayısının $1,5 \cdot 10^5$ değerinde deneysel olarak incelenmiştir. Bir küt cisim olarak kullanılan 25 mm çapındaki dairesel silindir, kanat profilinin iz bölgesinde akış yönünde aynı ekseninde yerleştirilmiştir. Boyutsuz boşluk S/D (burada S , kanat profili ile silindir arasındaki uzunlamasına boşluktur) ve kanat profili hücum açısı, α , sırasıyla 0° 'den $4,3^\circ$ 'e ve 0° 'den 15° 'ye kadar değiştirilmiştir. Kanat profili hücum açısının ve kanat profili ile silindir arasındaki uzunlamasına boşluğun basınç dağılımı ve girdap kopması üzerine etkileri incelenmiştir. Girdap oluşum bölgesi ve akış tutunması, tekrar tutunması ve ayrılma konumları, akış görüntüleme yardımıyla gözlenmiştir. Kanat profili ve dairesel silindirin önemli derecede birbirlerini etkiledikleri görülmüştür. Kanat profili hücum açısı ve uzunlamasına boşluk mesafesine göre akış yapılarındaki değişim, akış gözlem fotoğrafları kullanılarak açıklanmıştır.

Anahtar Kelimeler: Kanat profili, dairesel silindir, aerodinamik karakteristik, basınç dağılımı, Strouhal sayısı

*Corresponding author / Sorumlu yazar. Tel.: +90 462 3772959; e-mail/e-posta: sarioglu@ktu.edu.tr

1. INTRODUCTION

Circular and square cylinders are basic geometrical shape of bluff bodies and there are many studies and application areas. Flow control around the cylinder with the help of control rod [1-4], splitter plate [5-7] can be given as literature examples. Especially, flow around a circular cylinder has encountered in many engineering applications, for example, in the cooling tower, chimney and so forth. Sarioglu et al. [3] and Igarashi [8] investigated experimentally the effects of a thin rod having circular cross section, placed before a square cylinder in different distances, on the flow. They showed that there are two different flow structures depending upon the gap ratio between the two objects. Airfoil, as a streamlined or aerodynamic body, has also been used as a basic geometry in aerodynamics and hydrodynamics. Flow control around streamlined body by using a flap [9], dielectric barrier discharge (DBD) actuator [10] synthetic jet actuator [11] and so forth can be given as literature examples.

In the literature, there are many studies investigating flow structure of an airfoil. The wake of an airfoil usually includes instability waves and consistent structures with periodic indecisive motions, depending upon the Reynolds number and the angle of incidence. The NACA 0012 airfoil researched in this investigation is extensively used in aerodynamic applications. When flow structure of a single body compared with that of two objects in a uniform flow, it can be seen that there are considerable differences in terms of flow phenomena such as vortex shedding and fluctuating aerodynamic forces. Therefore, flow characteristic around two circular cylinders, two square cylinders and square and circular cylinder configuration in arranged tandem [12, 13], side by side [14], staggered [15] and combined [16] is widely available in literature. But streamlined and bluff body configuration in arranged side by side, tandem and so on is not studied widely in literature. In the following paragraphs, aforementioned type bodies' configuration in literature will be summarized.

Keser and Ünal [17] experimentally carried out a study on flow around a blunt-based flat plate at $Re_L = 1.46 \cdot 10^5$, $2.72 \cdot 10^5$ and $3.71 \cdot 10^5$ based on the plate length L . They measured the mean pressure distributions for the tandem and the staggered configurations that indicate different flow patterns depending upon gap ratios. Zhang et al. [18] examined the aerodynamic characteristics of a circular cylinder with an upstream NACA 4412 airfoil experimentally for $Re_d = 2100-20000$, based on the diameter of the cylinder, and $Re_c = 14700-140000$ based on chord length of the airfoil. They showed that while a lateral distance (T) increase, affected forces such as drag and lift suddenly decrease. They also revealed that Reynolds number of 60000 is critical value because of determined the vortex formation. While Re is smaller than 60000, vortex generation is occurred from airfoil.

Zhou et al. [19] numerically studied the effect of a circular cylinder in behind of NACA 4412 airfoil at Reynolds Number 200 based on the cylinder diameter. Their numerical study is divided into three groups, that is effects of attack angle, lateral spacing, and line distance, and are examined the vortex shedding and fluctuating forces. For the case of circular cylinder behind of NACA 4412 airfoil, while angle of incidence is bigger, vortex generation is decreased because of reattachment of separated shear layer from airfoil. Bajalan et al. [20] carried out an experimental study to investigate the effect of wake interaction of NACA 4412 airfoil and circular cylinder arranged in tandem with the help of hot wire anemometer. They indicated that circular cylinder placed behind the airfoil influenced the wake interaction and vortex formation region.

Henning et al. [21] investigated the aeroacoustic characteristic of the circular cylinder, that is used as control rod, in front of an airfoil. They measured the velocity field around this model by using particle image velocimetry and sound level by the means of phased-microphone array. They indicated that sound source is due to the leading edge of airfoil. Nakagawa et al. [22] performed an experimental study to investigate the effect of Mach number on flow around square cylinder placed in front of airfoil at Mach number changing between 0.15-0.9. They showed that vortex shedding around the model is not eliminated and also Strouhal (Sr) number is nearly constant up to $Ma = 0.7$, that is critical value, for the constant spacing ratio between cylinder and airfoil. After this critical Mach number, Airfoil placed behind the square cylinder influenced the flow structure. Imamura and Takahashi [23] numerically performed a study to investigate the effect of airfoil over noise production of circular cylinder arranged in side by side configuration. They showed that airfoil and the circular cylinder placed in side by side significantly affected the aerodynamic characteristic such as lift and drag forces, and aeroacoustic characteristic such as sound.

Munekata et al. [24] investigated the aeroacoustic characteristic such as sound generated from interaction of airfoil and circular cylinder arranged in tandem. Flow visualization and acoustic measurements are carried out for the airfoil placed behind circular cylinder. They showed that peak sound pressure level is changed periodically with gap ratio between airfoil and circular cylinder and also obtained three different flow modes based on gap ratio. Strouhal number increases with augmentation of gap ratio.

In the study of Percin et al. [25], time-dependent velocity fields or flow around NACA 0012 airfoil is obtained by using Particle Image Velocimetry. They showed that airfoil vibration characteristics can strikingly be changed depending upon locations of the downstream cylinder. The primary effect of the existence of the downstream

AERODYNAMIC CHARACTERISTICS OF THE FLOW AROUND AN AIRFOIL AND A CIRCULAR CYLINDER

cylinder is to diminish the amplitudes of high-frequency modulations. Yıldırım et al. [26] investigated the interaction of flow around circular cylinder placed in behind of an airfoil. Their results show vortex shedding from this configuration is affected by the position of the airfoil and a circular cylinder.

In this paper, an experimental study has been carried out for aerodynamics characteristics of the airfoil-cylinder combination. In this configuration, the important parameters chosen are the longitudinal spacing and attack angle of the airfoil. Because of separation on the airfoil depending on the attack angle, the changes in the pressure forces are very significant. For this reason, in this study it is aimed to give information of pressure fields around airfoil and cylinder about the structures of flow around the bodies measuring pressures on an airfoil and on a circular cylinder placed in tandem, and also making velocity–spectrum measurements in the wakes of the bodies. In the experiments, a circular cylinder as a bluff body and a symmetrical airfoil NACA 0012 as a streamlined body have been used. Experiments have been carried out at a Reynolds number of $1.5 \cdot 10^5$ based on the chord length of the airfoil, C (or at a Reynolds number of $2.5 \cdot 10^4$ based on the diameter of the circular cylinder, D). Angle of attack of airfoil was varied from 0 to 15 degrees while the dimensionless spacing was varied from 0 to 4.3. In this study, both the control of separation on the airfoil using a bluff body placed in the wake and also the effect of wake flow, produced from the airfoil, on the characteristics of a bluff body having circular cross section have been investigated for different values of the longitudinal spacing between the two bodies.

2. MATERIALS AND METHOD

The experiment study was performed at the low-speed, open-type wind tunnel. As shown in Figure 1, working section of this wind tunnel has measures 457 mm wide, 457 mm high, and 1830 mm long. At the maximum tunnel speed of about 36 m/s, the free stream turbulence intensity was about 0.5%; the turbulence intensity was higher at low tunnel speeds, about 1.5% at 5 m/s, which is the lowest speed in the tunnel. Experiments for pressure measurement have been carried out at a Reynolds number of $1.5 \cdot 10^5$ based on the chord length of the airfoil, C (or at a Reynolds number of $2.5 \cdot 10^4$ based on the diameter of the circular cylinder, D).

The configuration of the airfoil and a circular cylinder in tandem and the coordinate system are shown in Figure 2. The chord length of the symmetrical NACA 0012 airfoil, one of the basic airfoil geometries, C and the diameter of the circular cylinder tested, which was made of stainless steel, D , were 150 mm and 25 mm, respectively. The widths of the models used were 452 mm. The rotation center of the airfoil is 25 mm from the leading edge and 125 mm from the trailing edge. The angle of attack of the airfoil α defined in the Figure 2 is changed as $\alpha = 0^\circ, 5^\circ, 10^\circ$ and 15° in the rotation centre. The angle θ defined in the Figure 2 is the circumferential angle measured from the stagnation point on the cylinder. The experiments were carried out in the cases of $S/D = 0, 1, 2, 3, 4.3$. Here, the values of S/D are determined at $\alpha = 0^\circ$.

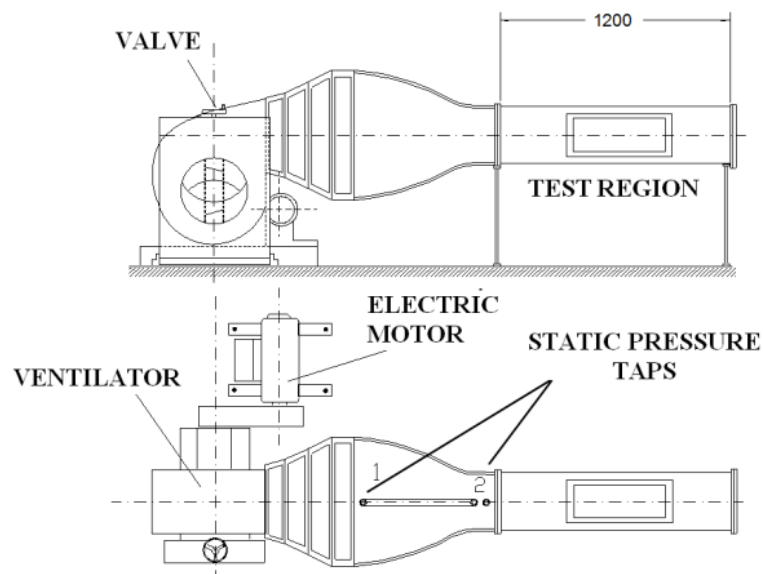


Figure 1. Low-speed, open-type wind tunnel and test section

M. SARIOGLU

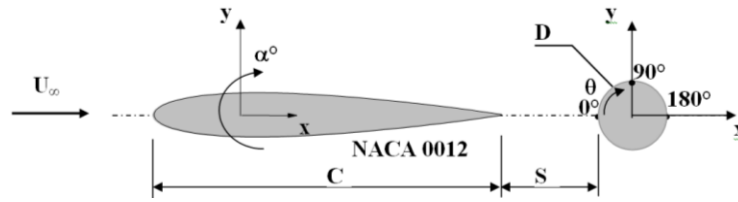


Figure 2. Flow configuration and symbol definition

For the pressure measurements, 12 pressure taps on the upper surface and 11 pressure taps on the lower surface of the airfoil and 1 pressure tap on the circular model have been used. Pressures on the circular cylinder have been measured by rotating it in steps of θ . The pressure taps have a diameter of 0.9 mm. The pressure measurements have been made on the middle sections of the models. In the pressure measurements, two pressure transmitters with a range of 0 to 50 and 0 to 75 mmSS in conjunction with a TSI Model 157 signal conditioner have been used. The transmitters were connected to the pressure taps in reference to the free stream wall pressure.

TSI IFA 100 model constant temperature anemometer (CTA) used in order to determine the Vortex shedding frequency from the airfoil and the cylinder. Two hot-wire probe were located at the positions of $x' = 5.5D$, $y' = 1D$ between the two bodies and $x = 2.5D$, $y = 1D$ in the downstream of the circular cylinder.

Velocity and pressure measurement data was collected as 2048 with the help of a computer-controlled data acquisition system. Data collection for velocity is carried out at sample frequency of 1 kHz using low-pass filter setting of 300 Hz. Data collection for pressure were performed at sample frequency of 200 Hz using low-pass filter setting of 100 Hz. TSI Thermal-Pro Software was used to obtain signals with a 12-bit A/D converter and obtain the statistical results of these signals.

The experimental uncertainties in the measurement of velocity, pressure and Strouhal number were determined to be less than $\pm 3.3\%$ and $\pm 6.7\%$ and ± 3.4 respectively. Blockage correction was not made because of flow asymmetry. The vortex shedding frequencies were determined from the spectral density distributions.

3. RESULTS AND DISCUSSION

3.1. Flow Visualization

Smoke-wire flow visualization experiment is performed to see the flow field around a symmetrical airfoil NACA 0012 and a circular cylinder at $Re_C = 3.6 \cdot 10^4$. Figure 3 shows flow phenomena such as flow separation, attachment and reattachments on the bodies. The variation of vortex formation region behind the bodies can be also appeared in this figure. When examined the photographs of the single airfoil, it is seen that wake region broadens with increasing α , whereas the airfoil has a narrow wake at $\alpha = 0^\circ$. In addition, in the cases of $S/D = 0$ and 2, the wake region broadens with increasing the attack angle and the flow separated from the surface of the airfoil reattaches on the surface of the circular cylinder.

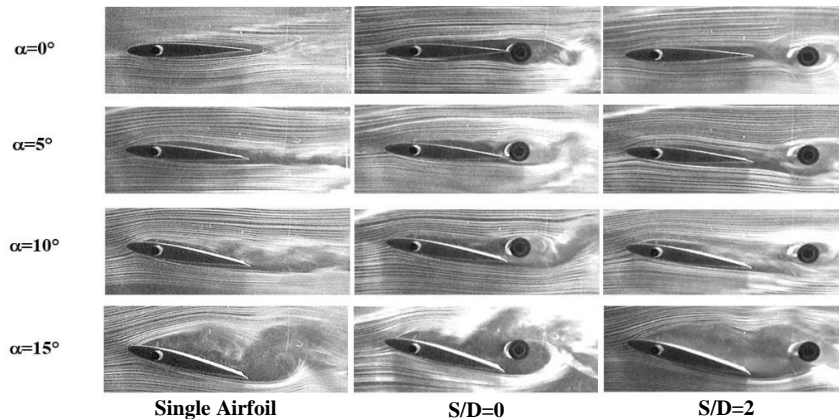


Figure 3. Smoke-wire visualization of the flow around the NACA 0012 airfoil and the circular cylinder in tandem for $Re_C = 3.6 \cdot 10^4$ ($Re_D = 6 \cdot 10^3$)

AERODYNAMIC CHARACTERISTICS OF THE FLOW AROUND AN AIRFOIL AND A CIRCULAR CYLINDER

3.2. Mean Pressure Distributions

Measurements of surface pressure were carried out on the surfaces of the NACA 0012 airfoil and the circular cylinder at the Reynolds number of $Re_c = 1.5 \cdot 10^5$ for $S/D = 0, 1, 2, 3, 4.3$ and for the attack angle of the NACA 0012 airfoil, α , in the range $0^\circ-15^\circ$ and the circumferential angle of the circular cylinder, α , in the range $0^\circ-360^\circ$ as shown in Figure 4-7. Pressure distributions were examined together with the visualization photographs. In the left side of the figures 4, 5, 6 and 7, pressure coefficient distributions on the upper and lower surfaces of the airfoil for the attack angles $0^\circ, 5^\circ, 10^\circ$ and 15° are given, whereas in the right side, pressure coefficient distributions measured on the circular cylinder placed behind the airfoil are given.

In Figure 4, in the case of $\alpha = 0^\circ$, it is seen that the values of pressures on the airfoil are affected slightly by the cylinder. It is well known that the pressure distribution is highest at the leading edge and decreases moving towards the trailing edge. Also, the pressure distribution is symmetrical on the airfoil NACA 0012 at $\alpha = 0^\circ$ and this means that lift force is zero. For the values of $S/D = 0$ and 1, there is a small increase in pressures on the rear region of the airfoil. In addition, the pressure distributions on the circular cylinder are favorably affected by the airfoil especially for the small values of S/D (0 and 1) in the case of the attack angle of $\alpha = 0^\circ$. Higher pressures than those in the case of bare cylinder occur specifically in the rear region. When examining the pressure distributions in Figure 4 together with the visualization photographs in Figure 3, it is possible to explain the flow structure at $\alpha = 0^\circ$ as follows: when the two body are in contact, that is $S/D = 0$, the boundary layer developed on the airfoil impacts to the front surface of the cylinder, whereas the shear layers above it pass from the bottom and upper surfaces of the circular model very closely. For this reason, a narrow wake is formed behind the circular model and this causes an increase in the base pressure of the cylinder. With increasing the longitudinal spacing between the airfoil and the cylinder, the flow structure changes and the shear layers separated from the upper and lower surfaces of the airfoil approach to the front surface of the circular cylinder as seen in the photograph for $S/D = 2$ in Figure 3. Accordingly, the pressure distribution at $S/D = 4.3$ is close to that in the case of the single cylinder.

When examined the pressure distributions on the airfoil in the case of $\alpha = 5^\circ$ (Figure 5), it is seen that there is a considerable increase in the pressure on the upper surface of the airfoil for $S/D = 0$ according to that in the case of the single airfoil. In this case, also there is important change on the lower surface. Here at $S/D = 0$, the cylinder impresses the flow passing under the airfoil, namely the boundary layer and causes negative pressures. That the pressure distributions on the lower surface become more negative means that the lift force working on the airfoil influences upside-down. Especially in this case, the shear layers passing over the airfoil reattach on the circular cylinder and consequently pressures increase in the region between the shear layer and the surfaces of the models. Thus, the pressure coefficient at rear point on the upper surface of the airfoil reaches to a value of +0.55. At the values of $S/D > 0$, the flow structure changes and the pressure distributions similar to those in the case of bare airfoil appear.

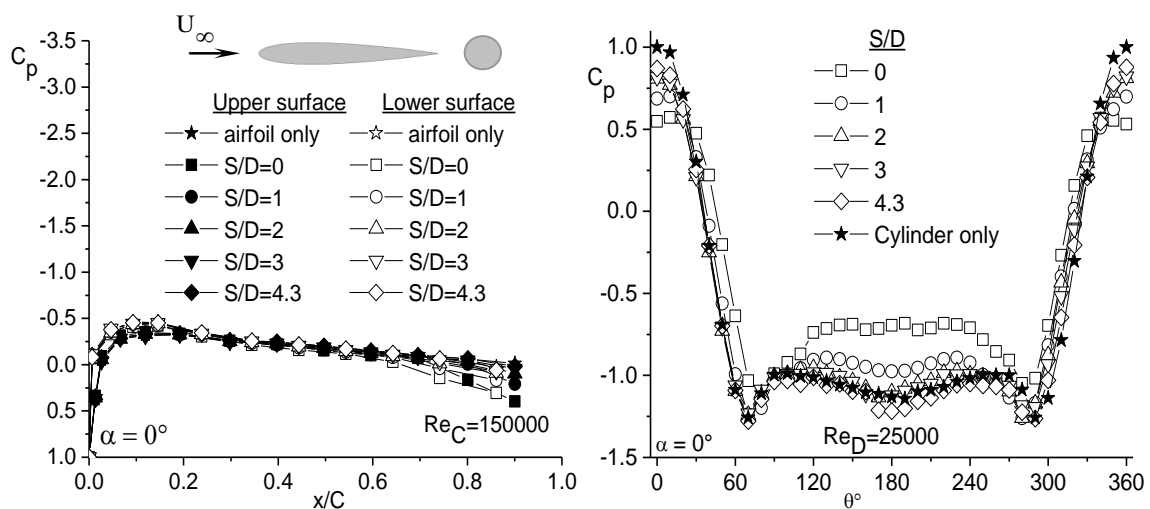


Figure 4 Pressure distributions on the NACA 0012 airfoil and the circular cylinder at $\alpha = 0^\circ$

In the case of $S/D = 0$, for $\alpha = 5^\circ$ the stagnation point on the cylinder occurs at approximately $\theta = 10^\circ$ and while the pressure value at the stagnation point for $\alpha = 0^\circ$ is about +0.5, it reaches to a value of +1.0 for $\alpha = 5^\circ$

M. SARIOGLU

in Figure 5. The pressures in the region of $\theta = 60^\circ$ - 240° on the circular cylinder for the case of $S/D = 0$ have higher values than those in the case of the single cylinder. Because, as seen in the photographs given in Figure 3 for $\alpha = 5^\circ$ and $S/D = 0$, the shear layers passing from the upper surface of the airfoil come by the upper surface of the cylinder and hence it is formed narrower wake region causing an increase in the base pressure. In return, as seen in the flow visualization photographs, due to the inclination of the airfoil ($\alpha = 5^\circ$), the shear layers following the lower surface of the airfoil pass lower of the cylinder according to the case of $\alpha = 0^\circ$ and therefore there is a decrease in pressures in the region $\theta = 260^\circ$ - 280° on the cylinder. With increasing S/D , the pressures on the surfaces of both the airfoil and the cylinder show similar patterns as in the case of single bodies. Especially, at the bigger values of S/D , the shear layers belong to the free stream passing over the airfoil may touch the cylinder. Here, the value of the stagnation point occurring at about $\theta = 0^\circ$ is 1.0.

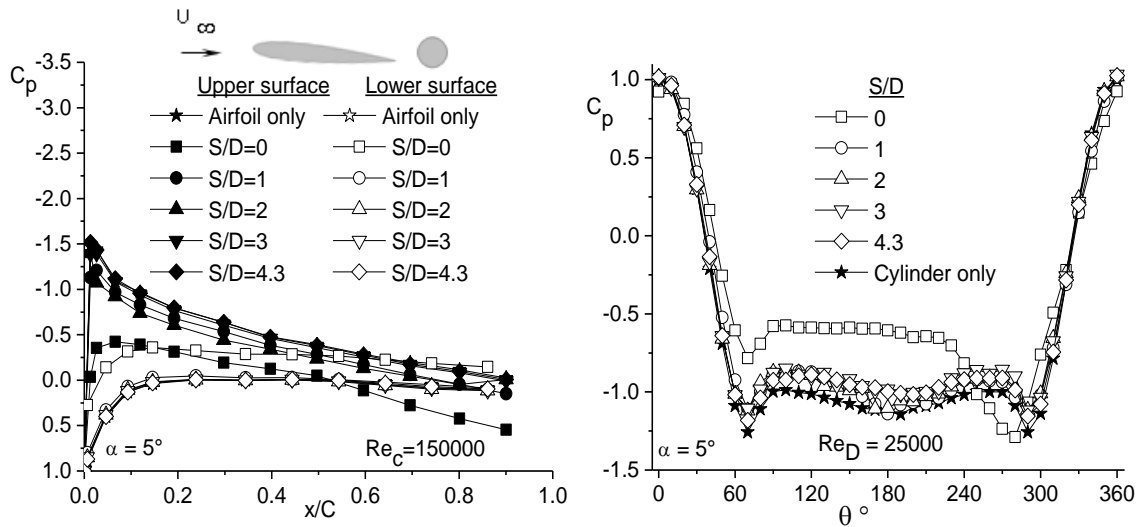


Figure 5. Pressure distributions on the NACA 0012 airfoil and the circular cylinder at $\alpha = 5^\circ$

In the case of $\alpha = 10^\circ$ in Figure 6, when examined the pressure distributions, the effect of S/D on the pressure distributions of the airfoil is little whereas pressure recovery occurs in the region $\theta = 60^\circ$ - 300° on the cylinder due to the effect of S/D . Because of increasing the velocity on the upper front region of the airfoil ($x/C = 0.0$ - 0.1), the level of pressure decreased considerably and this causes an increase in the lift forces. In the case of $\alpha = 10^\circ$ and $S/D = 0$, there is a base bleed flow which passes the gap between the trailing edge of the airfoil and the circular model, consequently the pressure distributions on the circular cylinder have a form similar to those of the single cylinder. Because of the attack angle of the airfoil, that is $\alpha = 10^\circ$, the flow coming from the upper side of the airfoil influences completely to the front region of the cylinder and hence for all S/D values, C_p at the front stagnation point of the circular model has a value of 1.0 as being in the case of the circular single cylinder.

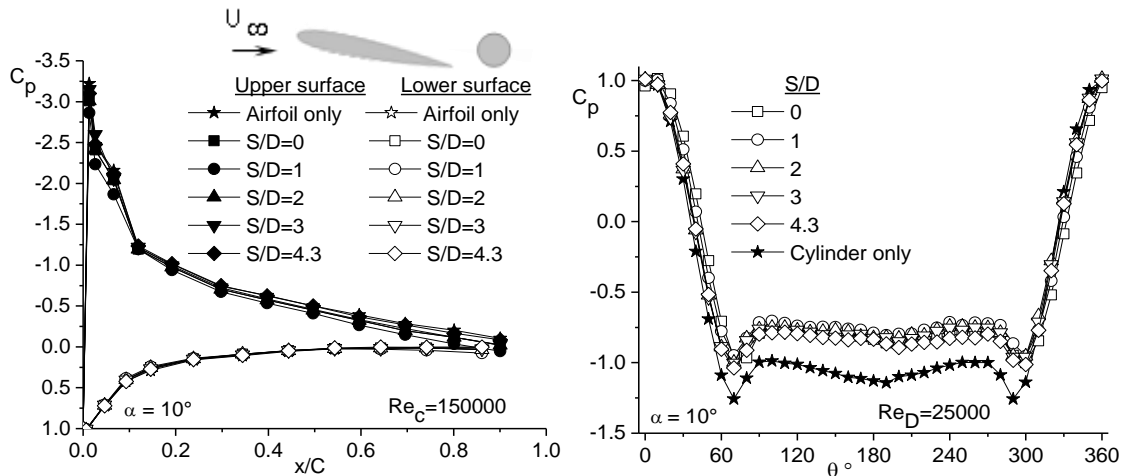


Figure 6. Pressure distributions on the NACA 0012 airfoil and the circular cylinder at $\alpha = 10^\circ$

AERODYNAMIC CHARACTERISTICS OF THE FLOW AROUND AN AIRFOIL AND A CIRCULAR CYLINDER

In Figure 7, in the case of $\alpha = 15^\circ$, both the pressure distributions of the airfoil and the circular cylinder have quite different characteristics according to those at smaller angles of attack. Because, at this attack angle, $\alpha = 15^\circ$, it occurs a wide wake region behind the airfoil owing to the onset of boundary layer from the upper surface of the airfoil. For all S/D values, while the pressures on the upper surface of the airfoil nearly coincide with those in the case of the single airfoil, these pressure values hardly change with x/C . Because the upper surface of the airfoil remains entirely in the wake region. Likewise, the pressures on the lower surface of the airfoil entirely coincide with those in the case of the single airfoil. Because the boundary layer belonging to the flow passing the lower surface has not been affected by the cylinder. When examined the pressures on the lower surface of the airfoil, depending on the attack angle having a big value, C_p gradually decreases from the stagnation point that the flow attaches to the surface. Here, the pressures become negative after $x/C = 0.35$ due to developing of the boundary layer. There is no separation from the lower surface of the airfoil but from the trailing edge. This fact is clearly seen in the flow photographs given in Figure 3 for the case of $\alpha = 15^\circ$, the single airfoil and $S/D = 0.0$ and 2.0 . Examining the pressures on the cylinder for $\alpha = 15^\circ$, while the pressure distributions for $S/D = 4.3$, the biggest value of S/D , and the single cylinder have same characters, the pressure coefficients for the values of $S/D < 4.3$ have completely different distributions. This shows two different flow structures.

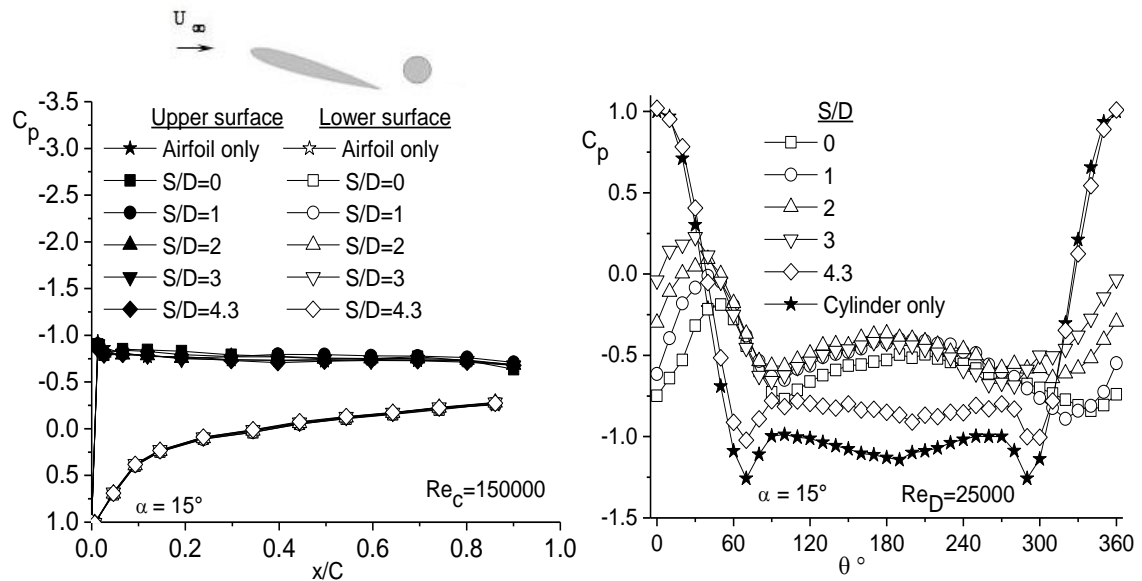


Figure 7. Pressure distributions on the NACA 0012 airfoil and the circular cylinder at $\alpha = 15^\circ$

In the flow structures in the range $S/D = 0.0-3.0$, the shear layers separated from the upper surface of the airfoil reattach on the circular cylinder. As the reattachment point occurs at $\theta = 50^\circ$ for $S/D = 0.0$, the angle of the reattachment point moves to the front side of the circular cylinder with increasing S/D and it occurs at $\theta = 30^\circ$ for $S/D = 3.0$. When S/D is increased from the value of 3.0 to 4.3 , the flow structure that the shear layer reattaches on the circular model changes and the circular cylinder remains in the vortex street produced by the rolling shear layers behind the airfoil. Thus, the circular model meets with an approaching flow having high turbulence, so the stagnation point occurs at $\theta = 0^\circ$ and C_p has a value of 1.0 . For $S/D = 4.3$, although the pressure distribution has a form similar to that of the single cylinder, as the flow has high turbulence the pressures on the rear surface of the circular cylinder are bigger than those of the single cylinder. For $S/D \geq 1.0$ at the angles of attack smaller than 15° , the pressure distributions have a concave shape in the middle in the range approximately $70^\circ-290^\circ$ on the surface of the circular cylinder. On the contrary, at $\alpha = 15^\circ$, they have convex distributions in the middle, except $S/D = 4.3$. As a matter of fact, examining the flow visualization photographs given in Figure 3, at the attack angle of 15° , the shear layer separated from the lower surface of the airfoil curls up due to the negative pressure in the wake and influences on the base region of the cylinder and thus causes the pressures in this region to increase.

3.3. Spectral Measurements and Strouhal Numbers

Spectra measured at range of Reynolds numbers between $6 \cdot 10^3$ and $4.4 \cdot 10^4$ are presented in Figure 8. They were obtained at the position $x'/D = 5.5, y'/D = 1$ between the airfoil and the circular cylinder for $S/D = 0, \alpha = 0^\circ$.

M. SARIOGLU

As shown in this figure, with increasing the Reynolds number, the shedding frequency increases from 32.23 Hz, in $Re = 6285$, to 240.23 Hz, in $Re = 44231$.

Spectral density distributions measured at different attack angles between $\alpha = 0^\circ-15^\circ$ for $S/D = 0$ and $S/D = 1.0$ are given in Figure 9 for $Re_D = 2.5 \cdot 10^4$. As shown in this figure, single peaks are obtained until $\alpha \cong 12^\circ$, while they are unapparent after approximately 12° . The shedding frequency remains nearly constant about 128 Hz until $\alpha \cong 12^\circ$.

Spectra measured at $x'/D = 5.5$ ve $y'/D = 1$ in the wake of the airfoil NACA 0012 between the two body in the range $\alpha = 0^\circ-15^\circ$ for $S/D = 0$ and $S/D = 1.0$ are given in Figure 10 for $Re_C = 1.5 \cdot 10^5$. Single dominant peaks are obtained until $\alpha = 12^\circ$ for $S/D = 0.0$, whereas they are obtained until $\alpha = 9^\circ$ for $S/D = 1.0$.

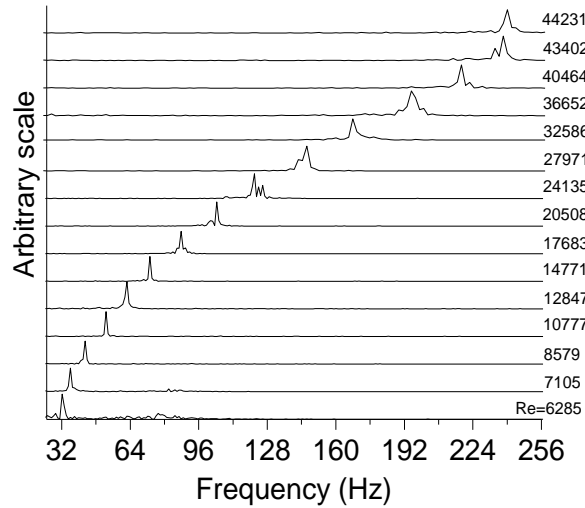


Figure 8. Spectra measured at $x'/D= 5.5$, $y'/D= 1$ between the airfoil and the circular cylinder for $S/D= 0$, $\alpha = 0^\circ$

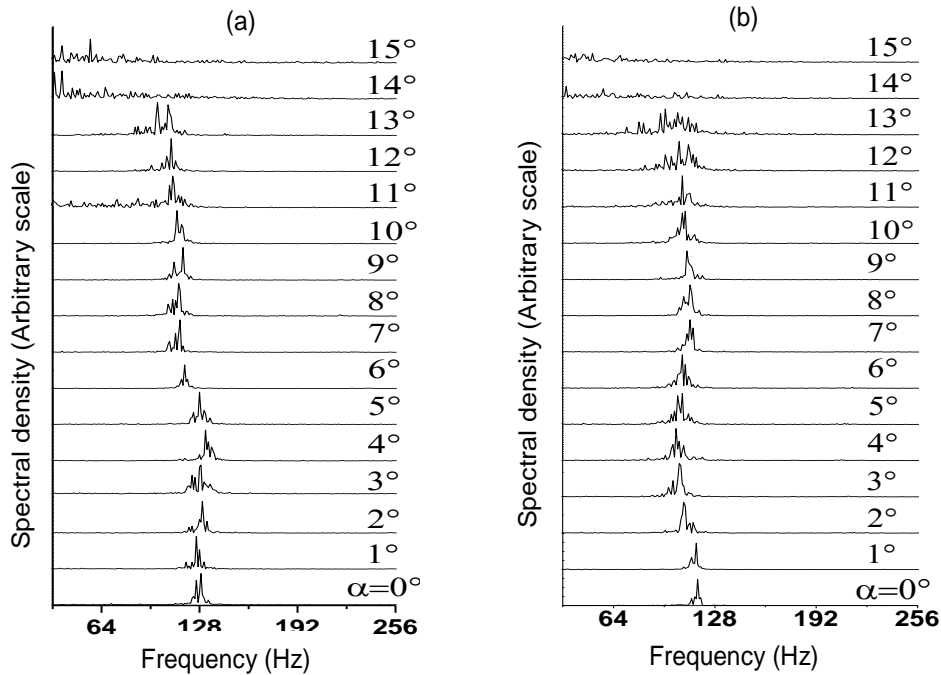


Figure 9. Spectra measured at $x/D = 2.5$ and $y/D = 1$ in the wake of the circular cylinder ($D= 25$ mm) in the range $\alpha= 0^\circ-15^\circ$ for (a) $S/D = 0$ and (b) $S/D = 1.0$

AERODYNAMIC CHARACTERISTICS OF THE FLOW AROUND AN AIRFOIL AND A CIRCULAR CYLINDER

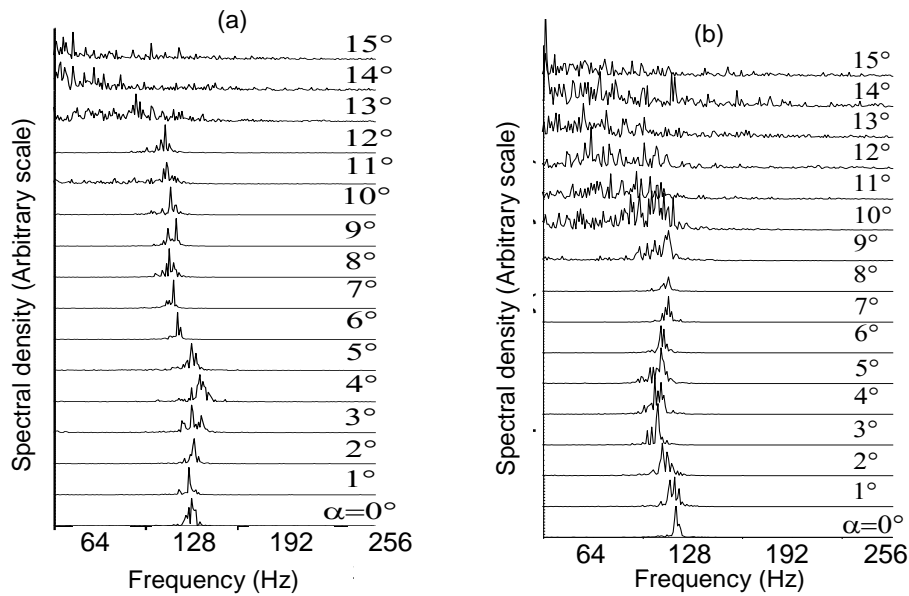


Figure 10. Spectra measured at $x'/D = 5.5$ and $y'/D = 1$ in the wake of the airfoil NACA 0012 (between the two body) in the range $\alpha = 0^\circ$ - 15° for (a) $S/D = 0$ and (b) $S/D = 1.0$

Strouhal numbers calculated using vortex shedding frequencies obtained from spectral distributions, versus Reynolds number for $\alpha = 0^\circ$ at different x-stations in the wake of the circular cylinder of diameter $D = 25$ mm and $D = 35$ mm are shown in Figure 11. In Figure 11a, which includes results of the circular cylinder of diameter $D = 25$ mm, there is a relatively small effect of Reynolds number on Strouhal number for $S/D < 3.0$. That is, with increasing the Reynolds number, the Strouhal number doesn't change considerably and it exhibits a distribution about the value of 0.20 for $S/D < 3.0$, whereas, it increases gradually with increasing the Reynolds number for $S/D = 3.0$ and 4.3 . In Figure 11b, which includes the results of the circular cylinder of diameter $D = 35$ mm, the Strouhal number increases continuously with increasing the Reynolds number for $S/D = 0.0$ - 3.0 . The Strouhal number for $S/D = 0.0$ has the bigger values according to those for the other S/D 's. The increase in Strouhal number with Re number is associated with the moving of the separation point to rear region on the cylinder due to high turbulent upcoming flow.

Strouhal numbers for different values of S/D are shown in Figure 12. As shown in this figure with increasing the attack angle of the airfoil, the Strouhal number is almost constant until 13° and then it sharply decreases. Here, it must be said that after this angle of 13° , stall starts. Until this angle, because the shear layers passing over the airfoil touch directly on the circular cylinder, it is obtained some explicit single peaks in the spectral distributions obtained in the wake of the cylinder. With increasing α , the airfoil creates a big projection height and thus it behaves as a bluff body having a wide wake region.

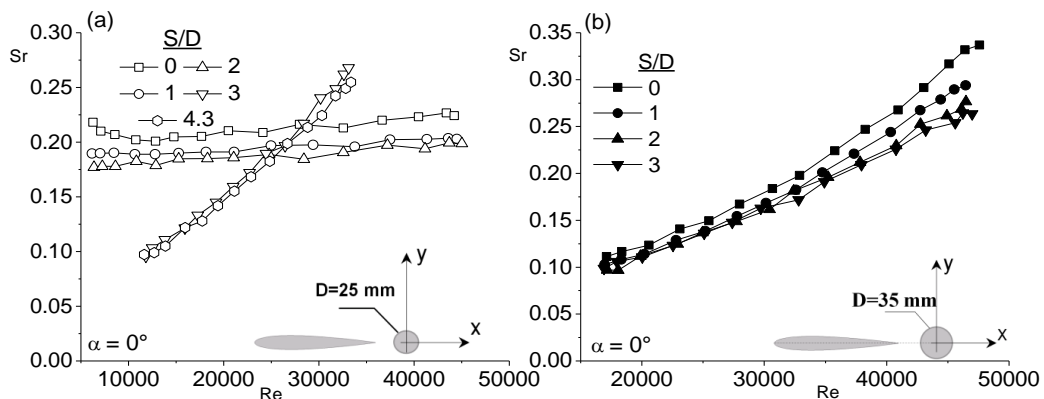


Figure 11. Strouhal numbers versus Reynolds number for $\alpha = 0^\circ$ (a) In the wake of the circular cylinder of diameter $D = 25$ mm at $x/D = 2.5$, $y/D = 1.0$ (b) In the wake of the circular cylinder of diameter $D = 35$ mm at $x/D = 2.5$, $y/D = 1.0$

M. SARIOGLU

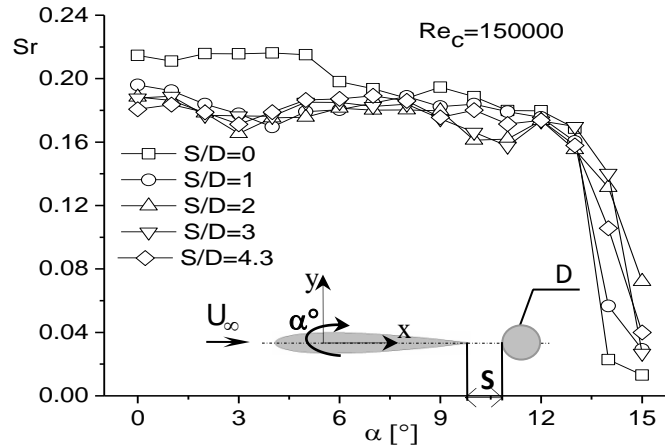


Figure 12. Strouhal number vs attack angle, α , at $x/D = 2.5$; $y/D = 1.0$ in the wake of the circular cylinder

In this case, the shear layers separated from the front upper and the back lower edge of the airfoil roll towards its wake having negative pressures and thus it is formed strong vortices behind the airfoil. In these attack angles, because the circular cylinder is completely in the wake region of the airfoil, the flow layers coming to the circular model are particularly comprised of these vortices. For this reason in these attack angles, in the spectral frequencies obtained behind the circular model, it is formed many weak peaks associated with the unsteady flow structure, where vortex shedding frequency of the airfoil is effective. While calculating the Strouhal numbers in Figure 12, the strong ones of these peaks are considered.

3.4. Drag Coefficients

As seen in Figure 13, variation of the drag coefficients of the cylinder as a function of S/D is plotted at the Reynolds number of $2.5 \cdot 10^4$. Drag coefficient is obtained from mean pressure measurement data. Here, drag results include the effect of the airfoil. As shown in this Figure, S/D has nearly no effect on the C_D for $\theta = 0^\circ - 10^\circ$, whereas, the drag coefficient increases gradually with S/D for $\theta = 15^\circ$. At $\theta = 0^\circ - 10^\circ$, because of the effect of the airfoil, the wake of the cylinder becomes narrower according to that of the bare cylinder. So, the increase in base pressure of the cylinder causes C_D to be lower than the value of about 1.2 of the bare cylinder. Also, as $\theta = 15^\circ$, because the cylinder remains entirely in the wake, pressures in front of the cylinder have negative values.

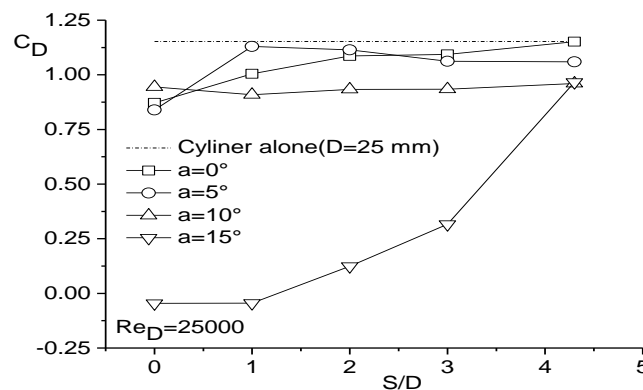


Figure 13. Drag coefficient on the circular cylinder of diameter $D= 25$ mm vs S/D

For this reason, especially in the cases of $S/D = 0$ and 1.0 , C_D has negative values, namely, thrust force acts to the cylinder instead of drag force. With increasing S/D , increase in the pressure of the front surface causes C_D to go up.

The drag coefficients of the circular cylinder versus α for different values of S/D are given in Figure 14. As shown in this figure, C_D remains almost constant until $\alpha = 10^\circ$ but decreases sharply after 10° for all of the values

AERODYNAMIC CHARACTERISTICS OF THE FLOW AROUND AN AIRFOIL AND A CIRCULAR CYLINDER

of S/D except for $S/D = 4.3$. For $S/D = 4.3$, the drag coefficient is nearly constant for all of the values of the attack angles considered.

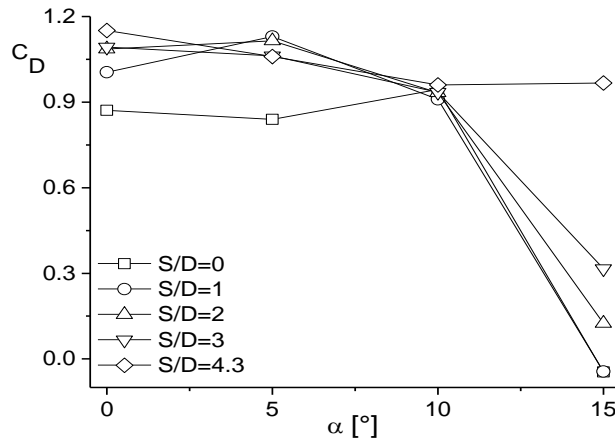


Figure 14. Variation of the drag coefficient of the circular cylinder of diameter $D= 25$ mm with α

4. CONCLUSIONS

The flow characteristics around a symmetrical airfoil NACA 0012 at incidence and a circular cylinder placed in tandem have been investigated experimentally. Pressure distributions of the models at $Re_C = 1.5 \cdot 10^5$ based on the chord length of the airfoil (C) and $Re_D = 2.5 \cdot 10^4$ based on the diameter of the cylinder (D) are obtained. The variation in the flow structures according to the attack angle of the airfoil and the longitudinal spacing between the airfoil and the cylinder are revealed utilizing the flow visualization photographs.

It is seen that in the case of $\alpha = 5^\circ$, for only $S/D = 0.0$, the pressures on the upper and the lower surfaces of the airfoil and the flow structure are different than those of the values of the single airfoil, while the pressures of the airfoil are not affected by the circular model in the case of $\alpha = 0^\circ$. In the case of $\alpha = 10^\circ$ and 15° , the pressure distributions of the airfoil are same with those of the single airfoil.

The pressure distributions of the circular cylinder have similar characteristics with those of the circular single cylinder at the attack angles of 0° , 5° and 10° but their values are a bit higher level. At the attack angle of $\alpha=15^\circ$, the pressure distributions for $S/D < 4.3$ have fairly different character according to the pressures of the circular model only and they have higher values at especially $\theta = 60^\circ-300^\circ$. It is seen that the flow structure for these small values of S/D causes the separated shear layer from the front upper edge of the airfoil to reattach on the surface of the circular cylinder between $\theta = 30^\circ-50^\circ$ and the separated shear layer from the back lower edge to increase the pressure in the region behind the circular cylinder.

In the spectra measured at the location $x'/D = 5.5$, $y'/D = 1$ between the airfoil and the circular cylinder for $S/D= 0$, $\alpha = 0^\circ$, with increasing the Reynolds number, the shedding frequency increases from 32.23 Hz, while the Reynolds number is 6285, to 240.23 Hz, while the Reynolds number is 44231.

With increasing the attack angle of the airfoil, the Strouhal numbers obtained behind the circular model remain nearly constant until $\alpha = 12^\circ$ because of hitting of the shear layers passing over the airfoil directly to the circular cylinder. The airfoil constitutes a wide wake region acting as a bluff body due to having a big projection height after $\alpha = 12^\circ$. For this reason, the vortex shedding structure of the circular cylinder is under the effect of the vortices created by the airfoil. For the circular cylinder of diameter $D = 25$ mm, there is a comparatively small effect of Reynolds number on Strouhal number for $S/D < 3.0$, whereas, the Strouhal number increases gradually with increasing the Reynolds number for $S/D = 3.0$ and 4.3 . But for the circular cylinder of diameter $D = 35$ mm, the Strouhal number continuously increases with increasing of the Reynolds number for $S/D = 0.0-3.0$.

REFERENCES

[1] LEE, S.J., LEE, S.I., PARK, C.W., “Reducing the Drag on a Circular Cylinder by Upstream Installation of a Small Control Rod”, Fluid Dynamics Research, 34, 233–250, 2004.

M. SARIOGLU

- [2] AKANSU, Y.E., OZMERT, M., FIRAT, E. “The Effect of Attack Angle to Vortex Shedding Phenomenon of Flow around a Square Prism with a Flow Control Rod”, *Journal of Thermal Science and Technology*, 31, 109–120, 2011.
- [3] SARIOGLU, M., AKANSU, Y.E., YAVUZ, T., “Control of the Flow around Square Cylinders at Incidence by Using a Rod”, *AIAA Journal*, 43, 1419–1426, 2005.
- [4] FIRAT, E., AKANSU, Y.E., AKILLI, H., “Flow Past a Square Prism with an Upstream Control Rod at Incidence to Uniform Stream”, *Ocean Engineering*, 108, 504–518, 2015.
- [5] AKANSU, Y.E., SARIOGLU, M., YAVUZ, T., “Flow around a Rotatable Circular Cylinder-Plate Body at Subcritical Reynolds Numbers”, *AIAA Journal*, 42, 1073–1080, 2004.
- [6] APELT, C.J., WEST, G.S., SZEWCZYK, A.A., “The Effects of Wake Splitter Plates on the Flow Past a Circular Cylinder in the Range $10^4 < Re < 5 \times 10^4$ ”, *Journal of Fluid Mechanics*, 61, 187–198, 1973.
- [7] SARIOGLU, M., AKANSU, Y.E., YAVUZ, T., “Flow around a Rotatable Square Cylinder-Plate Body”, *AIAA Journal*, 44, 1065–1072, 2006.
- [8] IGARASHI T., “Drag Reduction of a Square Prism by Flow Control Using a Small Rod”, *Journal of Wind Engineering and Industrial Aerodynamics*, 69, 141–153, 1997.
- [9] JANSEN, D.P., “Passive Flow Separation Control on an Airfoil-Flap Model”, Delft University, 2012.
- [10] AKANSU, Y.E., KARAKAYA, F., ŞANLISOY, A., “Active Control of Flow around NACA 0015 Airfoil by Using DBD Plasma Actuator”, *EPJ Web of Conferences.*, 45, 1008, 2013.
- [11] YOU, D., MOIN, P., “Active Control of Flow Separation over an Airfoil Using Synthetic Jets”, *Journal of Fluids and Structures*, 24 (2008) 1349–1357.
- [12] CHOI, C.B., JANG, Y.J., YANG, K.S., “Secondary Instability in the Near-Wake Past Two Tandem Square Cylinders”, *Physics of Fluids*, 24(2), 024102, 2012.
- [13] SOHANKAR, A., MOHAGHEGHIAN, S., DEHGHAN, A.A., DEHGHAN M., “A Smoke Visualization Study of the Flow over a Square Cylinder at Incidence and Tandem Square Cylinders”, *Journal of Visualization* 18, 687–703, 2015.
- [14] BURATTINI, P., AGRAWAL, A., “Wake Interaction between Two Side-by-Side Square Cylinders in Channel Flow”, *Computers & Fluids*, 77, 134–142, 2013.
- [15] ZHOU, Y., FENG, S.X., ALAM, M.M., BAI, H.L., “Reynolds Number Effect on the Wake of Two Staggered Cylinders”, *Physics of Fluids*, 21, 125105, 2009.
- [16] YAVUZ, T., AKANSU, Y.E., SARIOGLU, M., ÖZMERT, M., “Vortex Shedding on Combined Bodies at Incidence to a Uniform Air Stream”, *Proceedings of World Academy of Science Engineering and Technology*, 41, 1095–1099, 2009.
- [17] KESER, H.İ., ÜNAL, M.F., “Flow around a Circular Cylinder Downstream of a Blunt-Based Flat Plate in Tandem and Staggered Arrangements”, *Journal of Fluids and Structures*, 17, 783–791, 2003.
- [18] ZHANG, H.J., HUANG, L., ZHOU, Y., “Aerodynamic Loading on a Cylinder behind an Airfoil”, *Experiments in Fluids*, 38, 588–593, 2005.
- [19] ZHOU, C.Y., SUN, C.W., ZHOU, Y., HUANG, L., “A Numerical Study of a Circular Cylinder in the Wake of an Airfoil”, 15th Australas. Fluid Mech. Conf., Univ. Sydney, Aust., 2004.
- [20] BAJALAN, S., SHADARAM, A., HEDAYAT, N., TALEGHANI, A.S., “Experimental Study of Frequency Behavior for a Circular Cylinder behind an Airfoil”, *World Academy of Science, Engineering and Technology, International Journal of Mechanical, Aerospace, Industrial, Mechatronic and Manufacturing Engineering*, 5(11), 2356-2360, 2011.
- [21] HENNING, A., KOOP, L., EHRENFRIED, K., “Simultaneous Particle Image Velocimetry and Microphone Array Measurements on a Rod-Airfoil Configuration”, *AIAA Journal*, 48, 2263–2273, 2010.
- [22] NAKAGAWA, T., MEIER, G.E. A., TIMM, R., LENT, H.M., “Compressible Flows in the Wakes of a Square Cylinder and Thick Symmetrical Airfoil Arranged in Tandem”, *Proceedings of the Royal Society of London A: Mathematical, Physical and Engineering Sciences*, 411, 379–394, 1987.
- [23] IMAMURA, T., TAKAHASHI, Y., “Unsteady Flow Simulation around Cylinder under Airfoil Using Cartesian-Based Flow Solver”, *AIAA Computational Fluid Dynamics Conference*, 1–13, 2013.
- [24] MUNEKATA, M., KAWAHARA, K., UDO, T., YOSHIKAWA H., OHBA, H., “An Experimental Study on Aerodynamic Sound Generated From Wake Interference of Circular Cylinder and Airfoil Vane in Tandem”, *Journal of Thermal Science*, 15, 342–348, 2006.
- [25] PERCIN, M., TINAR, E., CETINER, O., UNAL, M.F., “Control of Self-Induced Pitching Vibrations of an Airfoil: Downstream Cylinder”, 12th International Symposium on Flow Visualization, German Aerospace Center (DLR), Göttingen, Germany, 2006.
- [26] YILDIRIM, I., CETINER, O., UNAL, M.F., “PIV Measurements of the Wake Interactions for a Circular Cylinder behind an Airfoil”, 6th International Symposium on Particle Image Velocimetry Pasadena, California, USA, 2005.